Thin-Walled Structures 190 (2023) 110971

Contents lists available at ScienceDirect

Thin-Walled Structures

journal homepage: www.elsevier.com/locate/tws

Full length article

Modeling of disc springs based on energy method considering asymmetric frictional boundary

Yanfeng Zhou [a], Dan Wang [a,*], Zhonghui Qiu [b], Zixiang Wei [a], Weifang Chen [a], Rupeng Zhu [a]

[a] National Key Laboratory of Science and Technology on Helicopter Transmission, Nanjing University of Aeronautics and Astronautics, Nanjing 210016, China
[b] Marine Engineering Gas Turbine Laboratory, No. 703 Research Institute, China State Shipbuilding Corporation, Harbin 150036, China

ARTICLE INFO

Keywords:
Disc springs
Frictional boundary
Mechanical model
Energy method
Structural parameters

ABSTRACT

Disc springs have excellent ability to absorb and dissipate energy, and are widely used as basic vibration isolation units in the design of vibration isolators for naval power systems. Focusing on the effect of friction on disc springs, a mechanical model of disc springs considering asymmetric frictional boundary is developed. The additional load to overcome the Coulomb friction damping is derived analytically by the energy method. Finite element analysis of disc springs is carried out and the results for large and small frictional conditions are compared with the theoretical results. Quasi-static experiments on disc springs are carried out and the proposed method is further validated. The results show that the analytical model based on energy method can describe the load–displacement characteristics of disc springs and their combinations under symmetric and asymmetric frictional boundaries accurately. Based on the analytical solution, the influence of the structural parameters of the disc springs on the damping effect is investigated. The stiffness and damping of disc springs are linearly related to the friction coefficient. In addition, the magnitude of the effect of asymmetry of the boundary friction on the mechanical properties of the disc springs varies with the structural parameters.

1. Introduction

Disc springs are compact elastic elements that provide excellent vibration isolation over a certain range of deformations [1]. In addition to single-piece use, multiple pieces of disc springs can be easily stacked in parallel or in series to form a combined vibration isolator [2]. Disc springs can also be combined with other components such as rubber and metal rubber to form hybrid vibration isolators, which can meet a wide range of vibration isolation stiffness and damping requirements [3–5].

Therefore, isolators composed of disc springs are widely used in aerospace, marine, automotive and construction applications [6]. Meng et al. [7] proposed a new quasi-zero stiffness vibration isolator by combining disc springs and vertical linear springs, and analyzed its dynamic characteristics. Ramhormozian et al. [8] pointed out that the use of disc springs can improve the shock resistance of sliding hinge joints and carried out an optimization study, including the optimal use of disc springs. Castagnetti et al. [9] designed an innovative energy converter based on electromagnetic vibrations using disc springs. Zhang et al. [10] designed a new disc brake for mine hoists based on disc springs, which can detect disc spring force and positive braking pressure in real time. Fang et al. [11] designed a self-centering rocking system using disc springs made of shape memory alloy, which has excellent fatigue and corrosion resistance and can safely prevent excessive swaying of bridge piers. Wang et al. [12] proposed a new type of disc spring compound vertical vibration isolation bearing in order to improve the vibration isolation performance of the traditional disc spring isolation bearings. Ha et al. [6] designed a new suspension system based on magnetorheological fluid using disc springs and applied it to the vibration control of military vehicles.

In the recent few decades, computer technology and finite element simulation software have been developed at a high speed, thus the research on disc springs can be divided into two main categories: theoretical model studies and simulation analysis. The idea of how to obtain the analytical solution of the load–displacement relationship for disc springs was first given by Timoshenko. Timoshenko suggested that the disc spring could be treated as a thin-walled part, assuming that the cross-section would not be deformed and rotate around its neutral point when the disc spring was compressed. Almen and Laszlo [13] pioneered the development of load–displacement analytical solutions for disc springs based on Timoshenko's theory. Their work has had a profound impact on subsequent research and until now many national standards still refer to the Almen-Laszlo's equation [14–17]. The damping of the disc springs mainly comes from the Coulomb friction at the contact boundary, and the frictional conditions have a significant effect on the load–displacement curves of the disc springs. Then, Curti et al. [18,19] derived the analytical solution of the load–displacement relationship

* Corresponding author.
E-mail address: wangdan_053@nuaa.edu.cn (D. Wang).

https://doi.org/10.1016/j.tws.2023.110971
Received 5 January 2023; Received in revised form 12 May 2023; Accepted 20 June 2023
Available online 8 July 2023

of the disc springs by establishing the moment balance equations and found that the cross-section does not necessarily rotate around the neutral point, and the exact location of the rotation center is related to the structure and material of the disc spring itself. But these analytical solutions cannot handle the case of asymmetric frictional conditions. Thus, based on the moment balance method, Mastricola et al. [2,20] extended the Curti's equation further to make it applicable in the case of asymmetric frictional conditions. The Mastricola's method can be used for single-piece disc spring under asymmetric frictional conditions and for multiple disc springs under symmetric frictional conditions, but still not for multiple disc springs under asymmetric frictional conditions. Chen et al. [21,22] obtained an improved theoretical model based on the Almen-Laszlo and Curti models by taking the contact stiffness, a nonlinear contact factor, into account.

Based on the classical disc spring theoretical model, scholars have also improved the theoretical model for different types of disc springs. Karakaya et al. [23] analyzed the load carrying capacity of composite disc springs with different cross-sections and performed the corresponding simulation calculations and experimental verification, which led to the optimization of disc springs. Patangtalo et al. [24] proposed a mathematical model of fiber-reinforced composite disc springs with spatially varying material properties and geometric nonlinearity to solve the problem of load calculation for disc springs of non-axisymmetric materials. Wang et al. [25] studied the preload problem of slotted disc springs, including theoretical modeling, simulation calculations and experimental validation, and proved that the accuracy of their model is higher. Foard et al. [26] improved the Almen-Laszlo model proposed for metal disc springs by considering the variation of elastic modulus and Poisson's ratio of the laminate in polar coordinates, enabling it to be used for the load calculation of polymer composite disc springs.

With the help of the finite element method (FEM), scholars are able to easily study the effect of structures and boundary friction on the mechanical properties of disc springs [27,28]. Zheng et al. [29] used the energy method to derive a theoretical model for disc springs under frictionless conditions and proved its accuracy to be higher than the Almen-Laszlo model by finite element simulation results. Zhu et al. [30] modeled the grooved disc springs based on the FEM and obtained the load–displacement and stiffness–displacement curves of disc springs with different groove configurations. Chaturvedi et al. [31] reported the effect of stepped cross-sections of disc springs with trapezoidal cross-sections on load–displacement and variable stiffness characteristics based on FEM results. Ozaki et al. [32] carried out a systematic investigation of the effect of frictional boundaries on the static deformation behavior of a conical disc spring under axial loading using the FEM.

Currently, although there are some analytical solutions for disc springs, they do not allow a comprehensive consideration of asymmetric frictional conditions and stacking configurations. Therefore, in this paper, based on the existing research, we propose a mechanical model based on the energy method that comprehensively considers the friction at each contact boundary under asymmetric frictional conditions. Then the FEM and experiment results are compared with the theoretical calculation results. Finally, the influence of the structural dimensional parameters of the disc spring on its stiffness and damping is analyzed.

2. Disc springs models considering asymmetric frictional boundary

2.1. Literature review

The load–displacement curve of a disc spring loaded axially is an important basis for analyzing its mechanical properties. Disc springs can be divided into two categories: those with bearing surfaces and those without bearing surfaces, and this paper is devoted to the study of disc springs without bearing surfaces. A typical disc spring structure without bearing surfaces is shown in Fig. 1(a), and existing theoretical models have been developed assuming that the cross section of a disc spring will not be deformed when it is compressed. Almen and Laszlo [13] were the first to give the theoretical model, which is also used by most standards, and they assumed that during compression the cross section of the disc spring rotates around its center of form. The relationship between axial load F_{ISO} and displacement δ of a disc spring is given in the standards [14–17] as follows

$$F_{\mathrm{ISO}}(\delta)=\frac{1}{1\mp f_{\mathrm{R}}}\left(\frac{4E}{1-\mu^2}\right)\left(\frac{t^4}{UD^2}\right)\left(\frac{\delta}{t}\right)\left[\left(\frac{h}{t}-\frac{\delta}{t}\right)\left(\frac{h}{t}-\frac{\delta}{2t}\right)+1\right] \quad (1)$$

where E is the modulus of elasticity, μ is Poisson's ratio, D is the outer diameter of the disc spring, d is the inner diameter of the disc spring, U is the structural coefficient related to D/d, t is the thickness, h is the cone height, f_{R} is the friction coefficient of the contact boundary and "−", "+ " represent the loading and unloading process respectively.

Observing Eq. (1), it can be found that it is composed of friction-related coefficient and the frictionless load–displacement relationship of the disc spring. Subsequently, Curti et al. [33] carried out further research on this basis and established moment balance equations. Studies have shown that Almen's assumption does not consistent with reality, the disc springs cross section should rotate around point O during the actual loading process, as shown in Fig. 1(b).

According to Curti's research [33], the position of point O can be determined by the following formula

$$c=a\left(\frac{\mu}{1-\mu}\right)\left(\frac{\rho^{\mu-1}-1}{1-\rho^{\mu}}\right) \quad (2)$$

where c is the distance from the rotation center O to the central axis of the disc spring, a, b are the outer radius and inner radius of the neutral plane respectively as illustrated in Fig. 1(a), and $\rho=a/b$ is the outer to inner radius ratio.

As a result, Curti et al. gave the load–displacement model for a single disc spring with no-friction condition

$$F_{\mathrm{nf}}(\delta)=\frac{\pi E\delta}{a^2}\left(\frac{\rho}{\rho-1}\right)^2\left[(h-\delta)\left(h-\frac{\delta}{2}\right)\left(\frac{\rho+1}{\rho-1}-\frac{2}{\ln\rho}\right)t+\frac{t^3}{6}\ln\rho\right] \quad (3)$$

Correspondingly, the frictionless stiffness and deformation energy of the disc spring are further obtained as

$$K(\delta)=\frac{\mathrm{d}F_{\mathrm{nf}}(\delta)}{\mathrm{d}\delta}=\frac{\pi E}{a^2}\left(\frac{\rho}{\rho-1}\right)^2\times\left[\left(h^2-3h\delta+\frac{3}{2}\delta^2\right)\left(\frac{\rho+1}{\rho-1}-\frac{2}{\ln\rho}\right)t+\frac{t^3}{6}\ln\rho\right] \quad (4)$$

$$W(\delta)=\int_0^{\delta}F_{\mathrm{nf}}(\delta)\mathrm{d}\delta=\frac{\pi E}{a^2}\left(\frac{\rho}{\rho-1}\right)^2\frac{\delta^2}{2}\times\left[\left(h-\frac{\delta}{2}\right)^2\left(\frac{\rho+1}{\rho-1}-\frac{2}{\ln\rho}\right)t+\frac{t^3}{6}\ln\rho\right] \quad (5)$$

Further, Curti et al. [34] took into account the frictional conditions at the contact boundary and gave a load–displacement model under symmetric frictional conditions

$$F_{\mathrm{Curti}}(\delta)=\frac{F_{\mathrm{nf}}(\delta)}{1\mp f_{\mathrm{R}}\frac{h-\delta+t}{a-b}} \quad (6)$$

Also based on the moment balance method, Mastricola et al. [20] improved Curti's model by extending its applicability to asymmetric frictional conditions and obtained the following analytical solution

$$F_{\mathrm{Mastricola}}(\delta)=\frac{F_{\mathrm{nf}}(\delta)}{1\mp\left\{\frac{[af_{\mathrm{a}}-bf_{\mathrm{b}}-c(f_{\mathrm{a}}-f_{\mathrm{b}})](h-\delta)}{(a-b)^2}+\frac{t(f_{\mathrm{a}}+f_{\mathrm{b}})}{2(a-b)}\right\}} \quad (7)$$

where f_{a} and f_{b} are the friction coefficients of the contact surfaces of the upper and lower edges of the disc springs, respectively.

Under symmetric frictional conditions, Eq. (7) can be simplified to the form of Eq. (6). Both Mastricola's method and Curti's method

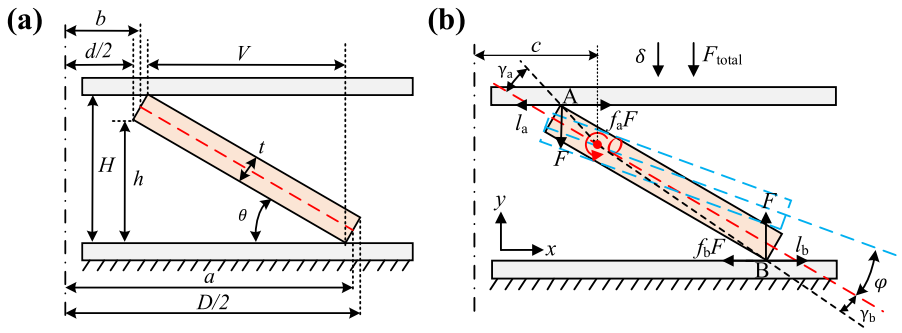

Fig. 1. Analysis model of a single disc spring: (a) structural dimensions of a single disc spring and (b) the deformation process of a single disc spring.

are based on the moment balance method and can be used to calculate the load–displacement relationship for single-piece disc spring under asymmetric frictional conditions and for multiple disc springs under symmetric frictional conditions, but still cannot calculate the load–displacement relationship for stacked disc springs under asymmetric frictional conditions [2,20]. In addition, when a large number of disc springs are stacked, it becomes very complicated and difficult to establish the moment balance equations.

Ozaki [32] proposed to use the energy method for the case of multiple disc springs stacked together by using Almen-Laszlo model as the master curve and obtaining the width of the load–displacement curve by calculating the energy loss due to friction. However, Ozaki's method is still based on the assumption that the disc spring cross section rotates around the form center and does not give specific expressions for the loading and unloading curves. Therefore, in this paper, based on Ozaki's method, a theoretical model of disc springs that considers asymmetric frictional conditions and stacking configurations is proposed.

2.2. Mechanical model for a single disc spring

The asymmetric frictional damping at the upper and lower contact boundaries during the deformation of the disc springs will produce energy loss. In order to overcome the Coulomb friction, the load at the same deformation during the loading process will increase. However, it is difficult to directly obtain the explicit relationship between the asymmetric frictional effect and the load increase, so it is a good choice to carry out the derivation of the analytical solution based on the conservation of energy.

When the disc spring is compressed, the work done by the outside world cannot be completely converted into deformation energy. To overcome the energy loss during compression, additional work needs to be done on the disc spring. According to the law of conservation of energy, there is

$$E^* = E_f + E_{\mathrm{I}} \tag{8}$$

where E^* is the additional work required, E_f is the energy dissipated by the Coulomb friction generated by the relative displacements between the upper and lower edges and the contact surfaces, and E_{I} is the internal energy dissipated by the disc spring during the compression process.

The dissipated internal energy can be calculated using the loss factor, and the loss factor is not only related to the material itself, but also affected by the working conditions. For metals, the loss factor is extremely small under low frequency and normal temperature conditions, so it can be considered that the internal energy dissipation is negligible [35]. Since the internal energy dissipation has little effect on the overall mechanical properties of the disc spring and is affected by many factors, it is ignored in this paper. In order to further reduce the influence of internal energy loss, the disc springs in this paper are all under quasi-static compression.

The energy dissipated by Coulomb friction during compression is

$$E = E_{f\mathrm{a}} + E_{f_{\mathrm{b}}} \tag{9}$$

where $E_{f\mathrm{a}}$ and $E_{f\mathrm{b}}$ are the energy loss caused by the friction of the upper and lower edges, respectively.

The additional work required by the disc spring can be written as

$$E^* = E^*_{f_{\mathrm{a}}} + E^*_{f_{\mathrm{b}}} \tag{10}$$

where $E^*_{f\mathrm{a}}$ and $E^*_{f\mathrm{b}}$ are the additional work required by the disc spring to overcome the friction of the upper and lower edges, respectively.

If the axial deformation load of the disc spring under frictionless condition is F, then the Coulomb frictional energy dissipation at the upper and lower edge contact surfaces during asymmetric frictional boundary loading is

$$\begin{cases} E_{f_{\mathrm{a}}} = f_{\mathrm{a}} F \mathrm{d}l_{\mathrm{a}} \\ E_{f_{\mathrm{b}}} = f_{\mathrm{b}} F \mathrm{d}l_{\mathrm{b}} \end{cases} \tag{11}$$

where l_{a}, $l_{\mathrm{b}}$are the slip distances at the upper and lower contact boundary, respectively.

The required additional work is

$$\begin{cases} E^*_{f_{\mathrm{a}}} = F^*_{f_{\mathrm{a}}} \mathrm{d}\delta \\ E^*_{f_{\mathrm{b}}} = F^*_{f_{\mathrm{b}}} \mathrm{d}\delta \end{cases} \tag{12}$$

where $F^*_{f\mathrm{a}}$, $F^*_{f\mathrm{b}}$are the additional loads required to overcome friction at the upper and lower contact boundary, respectively.

According to the principle of conservation of energy, there is

$$\begin{cases} E^*_{f_{\mathrm{a}}} = E_{f_{\mathrm{a}}} \\ E^*_{f_{\mathrm{b}}} = E_{f_{\mathrm{b}}} \end{cases} \tag{13}$$

The energy balance equations are established for the energy loss generated by friction, and the additional forces required to overcome the friction are obtained. The detailed derivation procedure is given in Appendix A, and the load–displacement relationship of a single disc spring for the asymmetric frictional conditions is

$$F_{\mathrm{single}}(\delta) = F \pm \left(F^*_{f_{\mathrm{a}}} + F^*_{f_{\mathrm{b}}} \right) = \left[1 \pm \frac{f_{\mathrm{a}} H_{\mathrm{a}} + f_{\mathrm{b}} H_{\mathrm{b}}}{V} \right] F_{\mathrm{nf}}(\delta) \tag{14}$$

where $H_{\mathrm{a}} = \mathrm{OA}\sin(\theta+\gamma_{\mathrm{a}})$, $H_{\mathrm{b}} = \mathrm{OB}\sin(\theta+\gamma_{\mathrm{b}})$, OA, OB are the lengths of the rotation arms from point O to the upper and lower contact points respectively, φ is the rotation angle of the cross section, θ is the base cone angle, γ_{a}, γ_{b} are the angles between OA, OB and the neutral plane respectively, and "+ ", "-" represent the loading and unloading process respectively.

From Eq. (14), it can be seen that the asymmetric frictional additional load is closely related to the upper and lower boundary friction coefficients. In particular, when the frictional effects of upper and lower contact surfaces are symmetric, i.e. $f_{\mathrm{a}} = f_{\mathrm{b}} = f$, Eq. (14) will be reduced to the symmetric friction form as

$$F_{\mathrm{single}}(\delta) = \left(1 \pm \frac{fH}{V} \right) F_{\mathrm{nf}}(\delta) \tag{15}$$

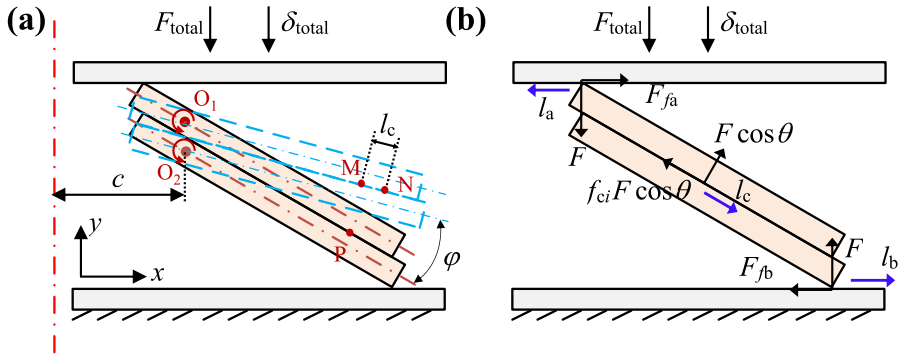

Fig. 2. Disc springs stacked in parallel: (a) working process and (b) analysis of the forces situation.

where H is the free height of disc spring, and V is the horizontal distance of contact points.

The stiffness and deformation energy of a single disc spring at the asymmetric frictional boundary are obtained by combining Eq.(14) and Eqs.(4) (5)

$$\begin{cases} K_{\text{single}}(\delta) = \left[1 \pm \frac{f_a H_a + f_b H_b}{V}\right] K(\delta) \\ W_{\text{single}}(\delta) = \left[1 \pm \frac{f_a H_a + f_b H_b}{V}\right] W(\delta) \end{cases} \tag{16}$$

2.3. Mechanical model for combined disc springs

Disc springs are often combined with multiple pieces as vibration isolation units in practical engineering applications, usually in the form of two combinations, parallel and series connections. The stiffness of disc springs in parallel and series stacks satisfies the laws of parallel and series connections, respectively, so that disc springs isolators with different mechanical properties can be obtained by using these two stacking methods appropriately. A parallel unit can be obtained by stacking several disc springs in parallel, and all combinations of disc springs can be seen as several parallel units connected in series.

Therefore, the analysis of disc springs stacked in parallel is carried out first. Assuming that the axial deformation of each single disc spring is δ, cross section rotation angle is φ, and axial deformation load is F. For the isolator with I disc springs stacked under frictionless condition, the axial total load is

$$F_{\text{total}} = IF \tag{17}$$

Taking the example of 2 disc springs stacked in parallel, as shown in Fig. 2. When disc springs are stacked in parallel, the displacement δ of each disc spring is the same as the displacement δ_{total} of the isolator. When the stacked disc springs isolator is subjected to axial load, in addition to the upper and lower contact boundaries, there will also be relative displacements and frictional effects on the stacked surfaces between the disc springs. Assuming that the two disc springs are rotated around $O_1(x_{O1}, y_{O1})$ and $O_2(x_{O2}, y_{O2})$ respectively during the deformation process, a contact point $P(x_P, y_P)$ on the stacked surface in the initial state is selected as the initial point, and $M(x_M, y_M)$, $N(x_N, y_N)$ are the positions of the corresponding points on the stacked surfaces after rotational deformation, respectively.

The distance l_c between points M and N is the deformed slip distance between the stacked surfaces, which can be expressed as

$$l_c = \sqrt{(x_M - x_N)^2 + (y_M - y_N)^2} \tag{18}$$

Extend to the case of multiple disc springs stacked in parallel. If a total of I disc springs are stacked, there are $(I-1)$ stacked surfaces, and the contact pressure on each stacked surface is $F_e = IF\cos\theta$. The frictional damping energy dissipated on all stacked surfaces is

$$E_{f_c} = \left[\sum_{i=1}^{I-1} f_{ci}\right] F_e \mathrm{d}l_c \tag{19}$$

where i represents the $i-$th contact surface, and f_{ci} is the coefficient of friction between certain stacked surfaces.

Similar to the case of a single disc spring, the frictional damping dissipation of the upper and lower contact surfaces, E_{f_a} and E_{f_b}, can be obtained separately. Correspondingly, the additional work required is

$$\begin{cases} E^*_{f_a} = F^*_{f_a}\,\mathrm{d}\delta \\ E^*_{f_b} = F^*_{f_b}\,\mathrm{d}\delta \\ E^*_{f_c} = F^*_{f_c}\,\mathrm{d}\delta \end{cases} \tag{20}$$

Also based on the law of conservation of energy, the energy balance equations are established

$$\begin{cases} E^*_{f_a} = E_{f_a} \\ E^*_{f_b} = E_{f_b} \\ E^*_{f_c} = E_{f_c} \end{cases} \tag{21}$$

With the above equations, the additional forces required to overcome friction when disc springs are stacked in parallel, $F^*_{f_a}$, $F^*_{f_b}$ and $F^*_{f_c}$, can be obtained. The specific formula derivation process is given in Appendix B, and the final load–displacement relationship for a parallel stack of I disc springs is

$$\begin{aligned} F_{\text{total}}(\delta_{\text{total}}) &= IF \pm (F^*_{fa} + F^*_{fb} + F^*_{fc}) \\ &= \left[1 \pm \frac{\left(\sum_{i=1}^{I-1} f_{ci}\right) t + f_a H_a + f_b H_b}{V}\right] I \cdot F_{\text{nf}}\left(\delta_{\text{total}}\right) \end{aligned} \tag{22}$$

By connecting several parallel units in series, a variety of disc springs isolators can be obtained. The disc springs isolator in Fig. 3 consists of a total of J parallel units, denoted as $S_j (j = 1, 2, \ldots, J)$. When the disc springs isolator is compressed, the displacement of each parallel unit is $\delta_j (j = 1, 2, \ldots, J)$. Based on the analytical solution under frictionless condition (Eq. (3)) and the series relationship, the relationship between δ_j and δ_{total} can be calculated. Based on the study of parallel stacking of disc springs, for any parallel unit S_j, the load–displacement relationship can be obtained

$$F_{S_j}(\delta_{S_j}) = I_{S_j} F_{\text{nf}-S_j}(\delta_{S_j}) \pm \left[F^*_{f_a-S_j}(\delta_{S_j}) + F^*_{f_b-S_j}(\delta_{S_j}) + F^*_{f_c-S_j}(\delta_{S_j})\right] \tag{23}$$

where I_{S_j} is the number of disc springs in the j-th parallel unit, $F_{\text{nf}-S_j}$ is the load of the j-th parallel unit under frictionless condition, and $F_{f_a-S_j}$, $F_{f_b-S_j}$, $F_{f_c-S_j}$ are the additional forces required by the $j-$th parallel unit to overcome the frictional dissipation at the upper contact, lower contact, and stacked surfaces, respectively.

Finally, the overall load–displacement relationship of the disc springs isolator can be obtained

$$F_{\text{total}}(\delta_{\text{total}}) = F_{S1}(\delta_{S1}) = F_{S2}(\delta_{S2}) = \cdots = F_{Sj}(\delta_{Sj}) \tag{24}$$

Table 1
Parameters of disc spring.

Outer diameter D/mm	Inner diameter d/mm	Thickness t/mm	Free height H/mm	Cone height h/mm
71	36	2.5	4.5	2.0

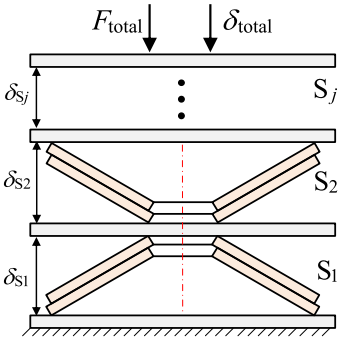

Fig. 3. Combined disc springs vibration isolator.

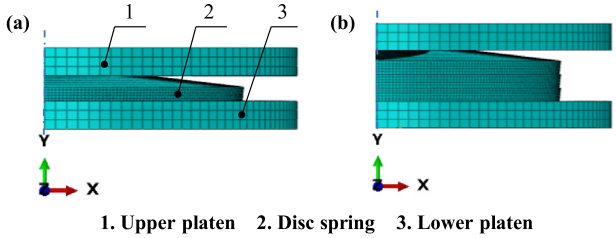

Fig. 4. Disc springs finite element models: (a) a single disc spring and (b) three pieces disc springs stacked in parallel.

In particular, when all disc springs in a vibration isolator consisting of J parallel units are of the same type and each parallel unit has I disc springs, Eq. (24) can be written in the following form

$$F_{\text{total}}(\delta_{\text{total}}) = \left[1 \pm \frac{\left(\sum_{i=1}^{(I-1)J} f_{ci}\right)\frac{t}{J} + \sum_{i=1}^{m} f_{ai}H_{\text{a}} + \sum_{i=1}^{n} f_{\text{b}i}H_{\text{b}}}{V}\right] I \cdot F_{\text{nf}}\left(\frac{\delta_{\text{total}}}{J}\right) \tag{25}$$

where m, n are the number of upper and lower contact boundaries respectively, and f_{ai} , f_{bi} are the $i-$th corresponding boundary friction coefficients.

3. Finite element simulation analysis

3.1. Finite element modeling

The finite element model including the upper and lower platens and disc springs is established, and the structural parameters of the selected disc springs without bearing surfaces are listed in Table 1.

Finite element analysis under quasi-static conditions using explicit method is performed in ABAQUS. In order to fully simulate the actual situation, the upper and lower platens and disc springs are modeled with deformed solids. The mesh size of each disc spring is 0.5 mm and the number of mesh elements is 72,360. The upper and lower platens have the same mesh division, the mesh size is 3 mm, and the number is 2058. The mesh element type of both disc springs and platens is C3D8R. The platens are made of structural steel material with a density of 7850 kg/m^3, the modulus of elasticity is 210 GPa, and Poisson's ratio is 0.31. The disc springs are made of 60Si2MnA, which has a density of 7850 kg/m^3, the modulus of elasticity is 206 GPa, and Poisson's ratio is 0.29.

The contact attribute adopts explicit general contact, the normal direction is hard contact, and the tangential direction adopts penalty function contact algorithm. Set the lower platen as a fixed restraint and apply displacement load to the upper platen. The axial (Y-axis) compression of a single disc spring is set to 1.8 mm ($0.9h$), and a complete loading and unloading process is calculated. Since no other friction is introduced when disc springs are stacked in series, the single-piece disc spring and the three-pieces stacked disc springs are mainly studied in the simulation analysis, and their finite element models are given in Fig. 4.

3.2. Finite element simulation results

In the solution process, in order to analyze the applicability of the energy method model for a single disc spring under different frictional boundary conditions, four contact boundary conditions are used: symmetric small friction (group ①), symmetric large friction (group ②), and asymmetric friction (groups ③ and ④).

When selecting a specific coefficient of friction, the following two factors are considered:

(1) The disc spring calculation formula in the standards [14–17] gives the recommended range of friction coefficient (<0.05), which is the low frictional condition;

(2) In actual engineering use, disc springs are usually placed between metal planes, and the friction coefficient is generally between 0.2–0.5 [36]. And as the metal rusts and wears, the coefficient of friction becomes larger, so the disc springs are more likely to be under high frictional conditions in practice.

The specific contact boundary friction coefficients are listed in Table 2. Compared with a single disc spring, when three disc springs are stacked in parallel, friction at the stacked surface of the disc springs will also be introduced. Similarly, the coefficients of friction for stacking disc springs are listed in Table 3.

When the friction coefficients at the upper and lower contact boundaries are symmetric (groups ① and ②), the results of the FEM, standards, energy method and moment balance method for a single disc spring are given in Fig. 5(a) and (b). The area enclosed by the loading and unloading curves is the frictional damping energy dissipated in loading–unloading cycle. Fig. 6 shows the errors of the standards, energy method and moment balance method with the FEM calculation results.

Overall, the calculation results of the standards are larger compared with the FEM results, and the error is more obvious especially under the large frictional condition. Under the small frictional condition (group ①), the errors between the maximum load of loading and unloading process obtained by standards with that obtained by the FEM are 9.85% and 8.99%, respectively. The relative error of damping is more obvious, but the actual difference is only 0.23J.

Under the large frictional condition (group ②), the load–displacement curve calculated by standards deviates seriously from the FEM curve. The error of the maximum load during loading process increased by 46.95%, but the error of the maximum load during unloading process did not change much. This also leads to a more significant increase in the damping error, which is 247.47% greater than in group ①. This is because the friction coefficient in group ② has increased to 0.3, which exceeds the recommended friction coefficient (<0.05) given in the standards, indicating that the standards are no longer applicable under large frictional conditions.

Table 2
Contact boundary friction coefficient of a single disc spring.

Group	Upper contact boundary friction coefficient f_a	Lower contact boundary friction coefficient f_b
①	0.02	0.02
②	0.3	0.3
③	0.02	0.3
④	0.3	0.02

Table 3
Contact boundary friction coefficient of combined disc springs.

Group	Upper contact boundary friction coefficient f_a	Lower contact boundary friction coefficient f_b	Friction coefficient of stacked surface f_c
⑤	0.02	0.02	0.2
⑥	0.3	0.3	0.2
⑦	0.02	0.3	0.2
⑧	0.3	0.02	0.2

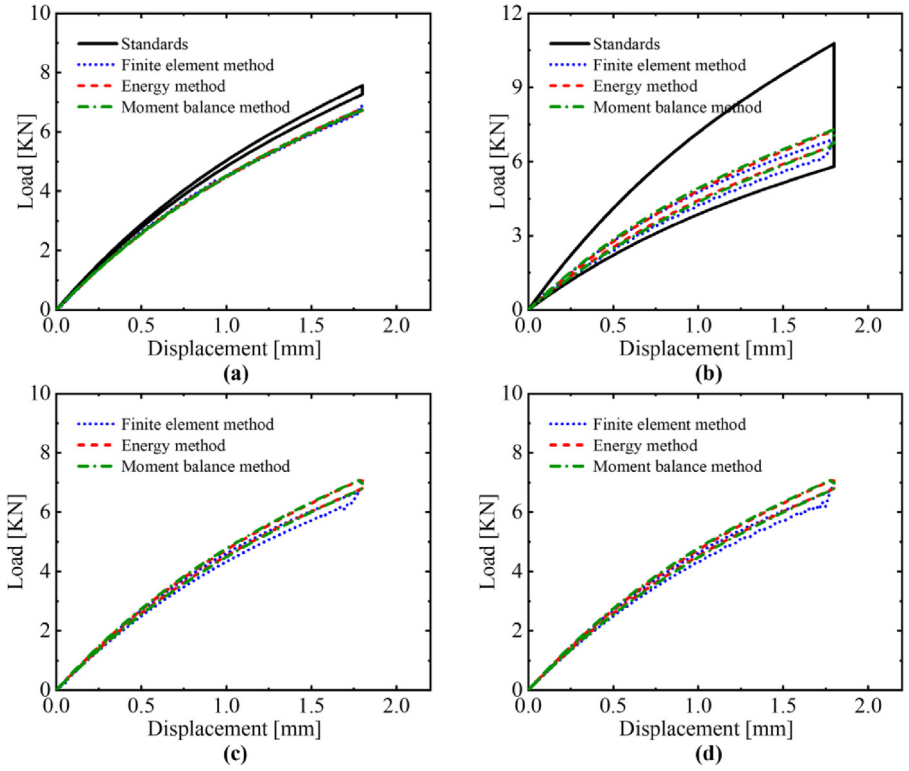

Fig. 5. Comparison of load–displacement curves of a single disc spring: (a) group ①; (b) group ②; (c) group ③ and (d) group ④.

The recommended range (<0.05) of the friction coefficient in the disc spring calculation formula is given in many national standards [14–17]. Based on the calculation results of FEM and moment balance method, it can be considered that the standards are more suitable for small frictional conditions. In addition, the standards are derived from Almen's research [13]. Curti et al. [37] demonstrated that Almen incorrectly used the assumption that radial stresses are negligible. Subsequently, Curti [19,33,34,38,39] verified the accuracy of the proposed new analytical formula through experiments and simulations, and scholars [1,2,20–22,30,40–42] generally recognized Curti's derivation process. Since the radial stress of the disc spring will inevitably increase under the condition of large friction, this may also lead to errors in the standards calculation results.

In groups ① and ②, the results of energy method and moment balance method are both in good agreement with the FEM results. Although the errors of maximum load of loading and unloading process also increased a little in group ② compared to group ①, they are maintained within 10%. The error in damping is slightly larger, but still within acceptable limits. This is because both methods perform quantitative analysis for the actual frictional effects, which effectively overcomes the applicability of the analytical solution under large frictional conditions and makes the accuracy of the calculation results improved.

The calculation results of different methods for asymmetric frictional condition (groups ③ and ④) are given in Fig. 5(c)–(d). Since the standards are not applicable to asymmetric frictional conditions, only the FEM, energy method and the moment balance method are included. It can be seen that both the energy method and the moment balance method can describe the hysteresis shape of the loading–unloading process very well. The errors with the FEM results are within 15% for both the maximum load during loading and unloading process, and the damping. During the loading–unloading process, the calculated loads of the energy method and moment balance method are slightly larger compared to the FEM results, probably because both methods are based on the assumption that the disc springs cross-section will not deflect, making the disc springs stiffer.

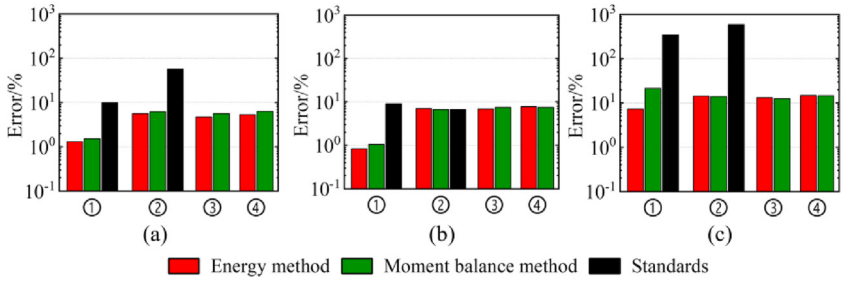

Fig. 6. Relative errors in the results of different methods and FEM for a single disc spring: (a) maximum load of loading process; (b) maximum load of unloading process and (c) damping energy dissipation in the loading–unloading cycle.

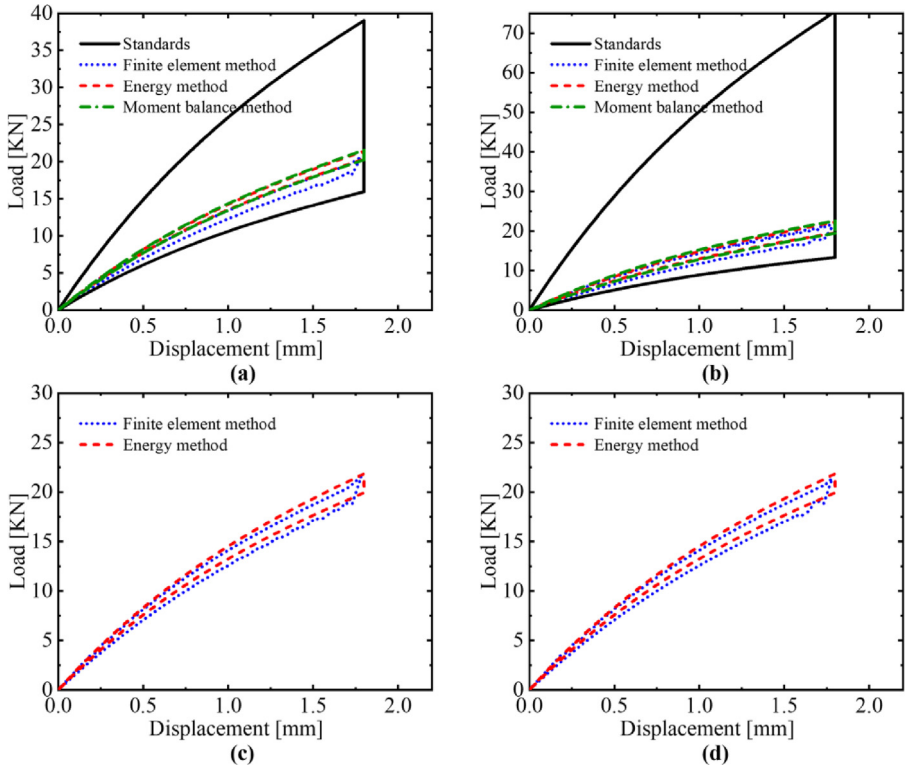

Fig. 7. Comparison of load–displacement curves of combination with 3 disc springs stacked in parallel: (a) group ⑤; (b) group ⑥; (c) group ⑦ and (d) group ⑧.

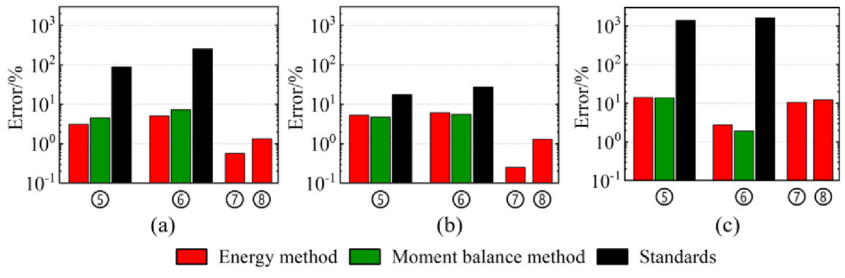

Fig. 8. Relative errors in the results of different methods and FEM for stacking disc springs: (a) maximum load of loading process; (b) maximum load of unloading process and (c) damping energy dissipation in the loading–unloading cycle.

Fig. 7 (a) and (b) show the results of the combination with 3 disc springs stacked in parallel for different symmetric frictional conditions (groups ⑤ and ⑥). Fig. 8 shows the errors between the maximum load of the loading and unloading process and damping calculated by different methods with the FEM results.

As can be seen, similar to the previous single-piece disc spring, the standards results are larger compared with the FEM results, and the error becomes more pronounced as the friction coefficient increases. When the friction coefficient increases, the error of the maximum load during loading process in group ⑥ increases by 168.23% compared with group ⑤. Analogous to the single disc spring, the change in the error of the maximum load during unloading process is smaller, increasing by only 10.08%. The error of damping in group ⑤ gets larger, becoming 3.99 times the error in group ①, and the error in group ⑥ increases further, reaching 1.12 times the error in group ⑤.

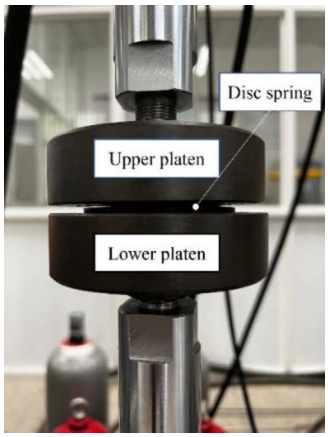

Fig. 9. Disc spring quasi-static compression experiment.

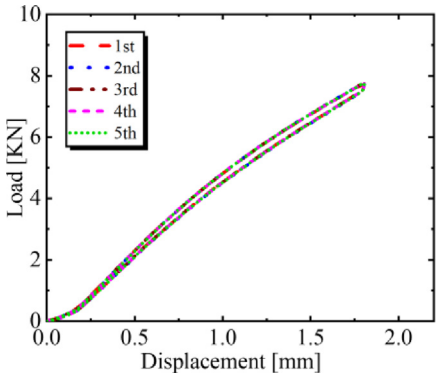

Fig. 10. Disc spring compression experiments under lubricated conditions.

This is because although the friction coefficient between the disc springs and the platens in group ⑤ is the same as in group ①, both are small frictional conditions, the coefficient of friction between the stacked surfaces of the disc springs is 0.2, which is still beyond the range recommended in standards. In group ⑥, the coefficient of friction between the disc springs and the platens is increased to 0.3, which further increases the error compared to group ⑤. In general, both the increase of friction coefficient between the disc springs and the contact surfaces and the increase of friction coefficient between the disc springs stacked surfaces can lead to an increase in the overall error of standards calculation results.

The energy method and the FEM results are in good agreement with both symmetric small and symmetric large frictional conditions. In both group ⑤ and group ⑥, the errors of the energy method and moment balance method are maintained at a low level, and the calculation results are able to capture the effects produced by the friction coefficient well.

For stacked disc springs, the moment balance method cannot yet be used for asymmetric frictional conditions (group ⑦ and group ⑧), so only the results of the FEM and the energy method are used in Fig. 7(c)–(d). Observing the whole loading–unloading cycles, we can find that the hysteresis characteristics are also well described under asymmetric frictional conditions. Compared with the FEM results, the errors of the maximum load during loading and unloading process obtained by the energy method in both group ⑦ and group ⑧ are less than 2%, and the errors of the damping are less than 15%.

4. Experimental verification

In order to verify the validity and accuracy of the energy method, the quasi-static compression experiments of disc springs are performed on the tensile and compression test machine shown in Fig. 9. The disc springs are placed between the upper and lower platens, where the movement of the upper platen can be controlled, while the lower platen is connected to a force sensor. By processing the collected data, we can obtain the full-range load–displacement curves of the disc springs.

To verify the accuracy of the energy method under asymmetric frictional conditions, four friction configurations as shown in Table 4 are prepared for the experiments. The "low" frictional condition is obtained by lubricating the contact surface with grease, and the "high" frictional condition represents the contact surface without lubrication. The damping grease is viscous and stable in nature, which makes the working process smoother and suitable for low speed and heavy load working conditions. We take the same mass of damping grease each time to lubricate the surface of the platen and apply it evenly. In addition, in order to prove the consistency, we did 5 experiments under lubricated conditions as shown in Fig. 10, and the load–displacement curves of the disc springs can overlap, so it can be considered that the consistency can be guaranteed. When large frictional condition is required, we use alcohol to wipe off the damping grease and clean the surface of the platen. The surface of the platen itself is a high frictional surface. Therefore, the consistency of the large frictional condition is much easier to ensure.

The friction coefficient is not only related to the surface roughness of the platen, but also to the material of the platen and the disc spring, which is difficult for us to measure by conventional methods. Since other influencing factors are ignored in this paper, it is considered that the damping of the disc spring is only produced by friction, so we use the combination of finite element calculation and experiment to fit the friction coefficient. Disc springs in Table 1 are used, and the specific process is as follows:

(1) In configuration I, a complete loading–unloading experiment is performed on a single disc spring, and the area S_L enclosed by the load–displacement curve is calculated;

(2) In configuration II, a complete loading–unloading experiment is performed on a single disc spring, and the area S_H enclosed by the load–displacement curve is calculated;

(3) In configuration II, a complete loading–unloading experiment is performed on two-pieces stacking disc springs, and the area S_P enclosed by the load–displacement curve can be calculated;

(4) Conduct FEM calculations for the loading–unloading experiments on a single disc spring and obtain the area S according to the load–displacement curve; low friction coefficient f_L is obtained when $S = S_L$; high friction coefficient f_H is obtained when $S = S_H$;

(5) Conduct FEM calculation for the loading–unloading experiment of two-pieces stacking disc springs, set the friction coefficient of the platen to f_H, and get the area S according to the load–displacement curve. When $S = S_P$, the friction coefficient f_P between the stacked surfaces of the disc springs can be obtained.

By comparing the damping in experiments with that of the FEM, the coefficient of friction is calculated to be 0.290 for "high" frictional condition and 0.095 for "low" frictional condition. In addition, the coefficient of friction between the contact surfaces of the disc springs is calculated to be approximately 0.151.

In order not to lose generality, another type of disc spring is selected to compare the load–displacement curves calculated by the energy method with experiment results, the specific dimensional information of which is listed in Table 5.

The load–displacement curves for a single disc spring in different friction configurations are shown in Fig. 11. From the shape of the hysteresis curves, it can be seen that the energy method is able to obtain the trend of the disc spring load–displacement curves under different frictional conditions. Especially, at the error evaluation point of $0.75h$ compression magnitude, the energy method results and the experimental results are in good agreement. For the asymmetric frictional conditions, the hysteresis curves are slightly wider in the III condition

Table 4
Different friction configurations.

Friction configurations	Upper platen frictional condition	Lower platen frictional condition
I	Low	Low
II	High	High
III	Low	High
IV	High	Low

Table 5
Structural parameters of the experimental disc spring.

	D/mm	d/mm	t/mm	h/mm	H/mm
Theoretical dimension	56	28.5	2	1.6	3.6
Measured dimension	55.76	28.77	1.95	1.63	3.56

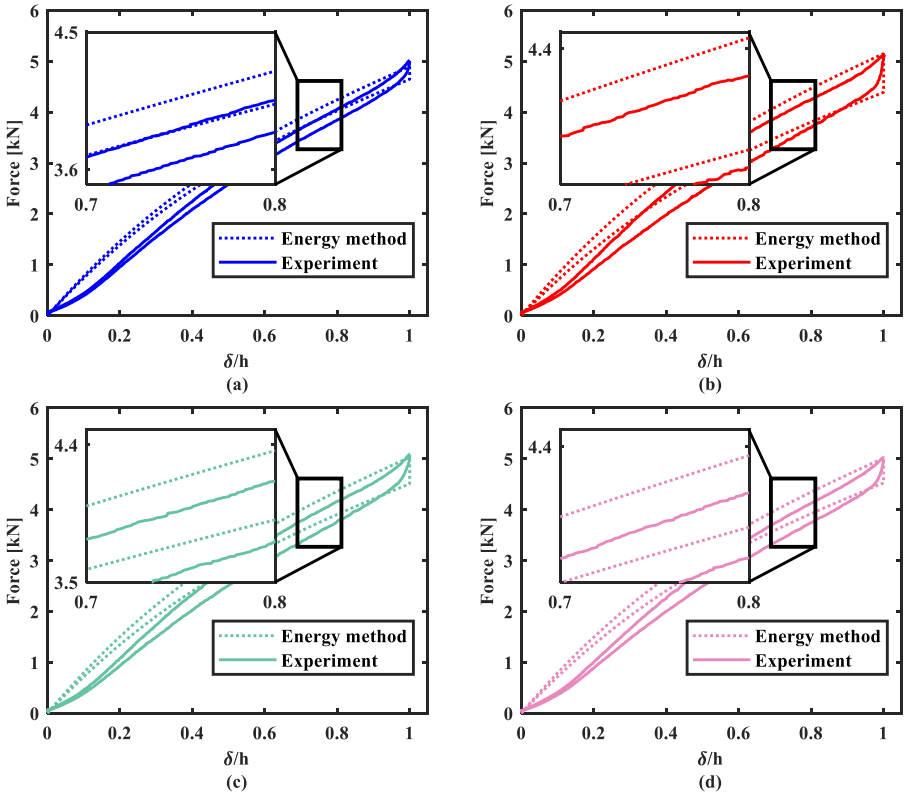

Fig. 11. Load–displacement curves under different frictional conditions.

Table 6
Disc spring damping in different friction configuration.

Friction configurations	Experimental results/J	Energy method results/J	Error/%
I	0.2577	0.2339	−9.24
II	0.7076	0.7147	+0.92
III	0.5023	0.4905	−2.35
IV	0.4653	0.4575	−1.68

than in the IV condition, and the results of the energy method can also reflect this feature.

The damping of the disc springs is presented in Table 6. The analysis of the damping shows that the calculated results of the energy method under both symmetric and asymmetric frictional conditions are very close to the experimental results, which proves the validity of the energy method under asymmetric frictional conditions. The relative error in the small frictional condition II is larger, which is due to the smaller absolute value of its damping.

The single-piece disc spring, double stacked disc springs and three stacked disc springs are tested separately, the load–displacement curves obtained from quasi-static compression experiments with different stacking configurations in symmetric friction configuration II are shown in Fig. 12, and the damping calculated by energy method is listed in Table 7.

For different stacking configurations, the load–displacement curves calculated by the energy method are in good agreement with the experimental curves, indicating that the energy method can describe the trend of the load–displacement curves of stacked disc springs. At the same time, we can find that the load–displacement curve obtained by the energy method for a single disc spring is closer to the experimental result. As the number of disc springs increases, the small stiffness region in the front part of the experimental curves becomes more and more obvious. This is due to the fact that disc springs may have small gaps between the stacked surfaces when they are stacked, so the stacked

Table 7
Disc spring damping in stacking configurations.

Stacking configurations	Experimental results/J	Energy method results/J	Error/%
A single piece	0.7076	0.7141	+1.00
Double pieces	1.8415	1.8329	−0.47
Three pieces	3.7658	3.3563	−10.87

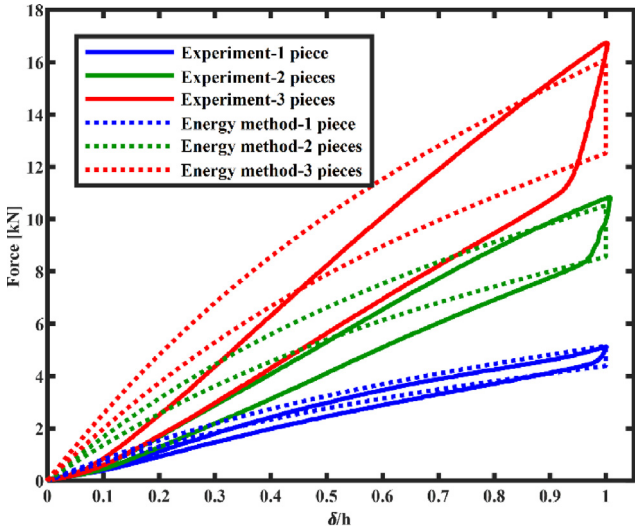

Fig. 12. Load–displacement curves of different stacking configurations: (a) experimental results and (b) energy method results.

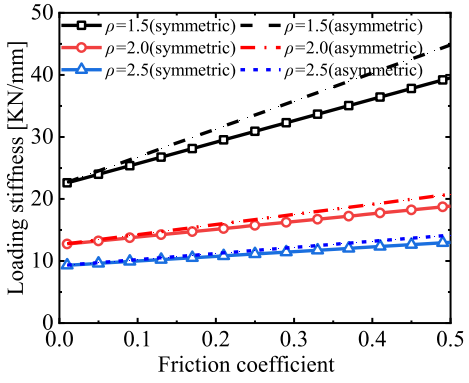

Fig. 13. The change of loading stiffness with friction coefficient under different ρ.

disc springs as a whole will exhibit less stiffness at the beginning of compression.

In terms of damping, the energy method also has good accuracy. When disc springs are used in stacks, Coulomb friction between the stacked surfaces is introduced, resulting in an overall increase in damping. As the number of stacked disc springs increases, the overall damping does not increase linearly. It can be seen that there is a great increase in damping when three disc springs are stacked, and the energy method successfully captures this changing characteristic. When the three disc springs are stacked, the damping error obtained by the energy method is 10.87%. However, it is worth noting that as the number of disc springs stacked increases, the damping error calculated by the energy method also increases. This may be due to the deflection of the cross section of the disc springs in actual compression, which leads to an increase in the relative displacements between the stacked surfaces. Although this is not consistent with the assumptions made in the establishment of the theoretical model, it is difficult to take into account.

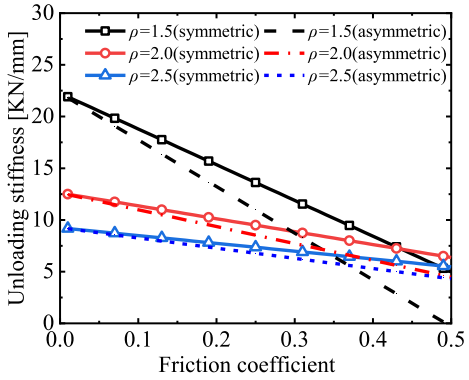

Fig. 14. The change of unloading stiffness with friction coefficient under different ρ.

5. Analysis of the influence of structural parameters on frictional effects

This section investigates the influence of each structural parameter (ρ, t, h) on the frictional effect of disc springs based on the analytical solution obtained by the energy method. The higher the number of disc springs stacked, the more pronounced the influence of structural parameters arises. For the convenience of observation, an analytical model of combination with 6 disc springs stacked in parallel is established. Set $f_a = f_b = f_c = f$(symmetric) and $f_a = 0.5f$, $f_b = f$, $f_c = 1.5f$ (asymmetric) frictional conditions, keep the outer diameter of the disc spring unchanged, and set different structural dimension parameters.

5.1. Analysis of the effect of ρ on friction

The relationship between stiffness (loading and unloading), damping dissipation and friction coefficient for different ρ at $0.75h$ is shown in Figs. 13–15. It can be seen that for an arbitrary ρ, with the increase of the friction coefficient, the loading stiffness gradually increases, the unloading stiffness gradually decreases. As a result, the width of the hysteresis curve becomes larger, indicating the damping energy dissipation gradually increases, and the curves under symmetric and asymmetric frictional conditions show an obvious linear trend.

The slopes of the curves of stiffness and damping dissipation with the friction coefficient for different ρ are shown in Fig. 16. It can be seen from the figure that the absolute value of the slope of the change in stiffness and damping dissipation energy gradually decreases as ρ increases, indicating that the sensitivity of stiffness and damping dissipation energy to the friction coefficient is lower at large ρ. The asymmetry of the boundary friction increases the absolute value of the slope of the stiffness and damping dissipation change for different ρ, and the larger the ρ, the smaller the increase magnitude.

5.2. Analysis of the effect of t on friction

The relationship between stiffness (loading and unloading), damping dissipation and friction coefficient for different t of disc springs at $0.75h$ is shown in Figs. 17–19. Similar to the effect caused by ρ, it can be seen that for any t, as the friction coefficient increases, the loading stiffness gradually increases, the unloading stiffness gradually decreases, and the damping energy dissipation gradually increases.

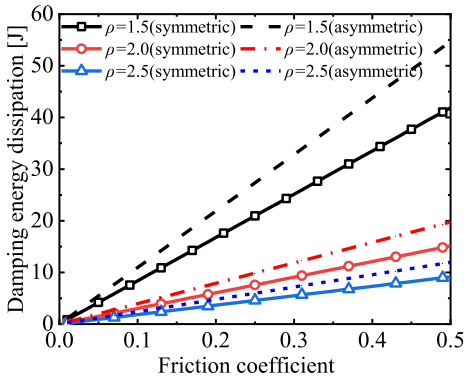

Fig. 15. The change of damping energy dissipation with friction coefficient under different ρ.

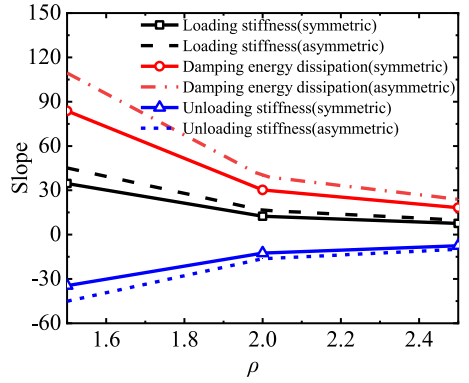

Fig. 16. Loading, unloading stiffness and damping energy slope change with the change of ρ.

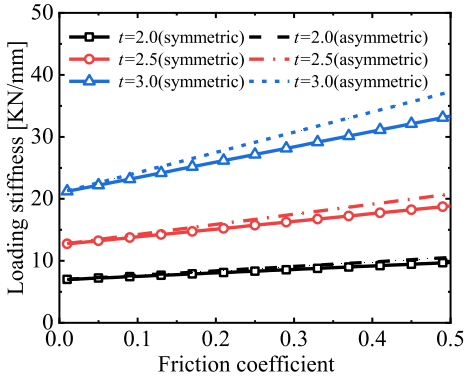

Fig. 17. The change of loading stiffness with friction coefficient under different t.

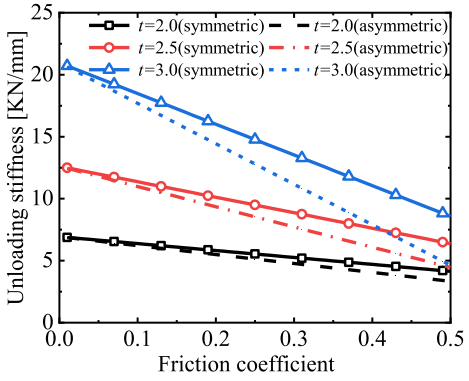

Fig. 18. The change of unload stiffness with friction coefficient under different t.

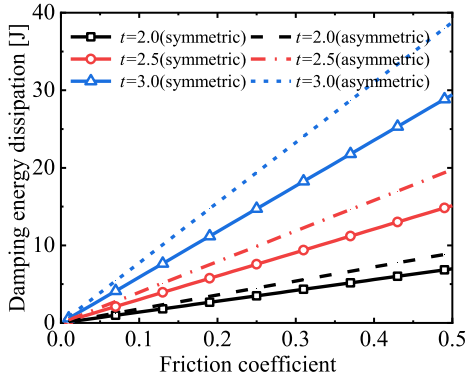

Fig. 19. The change of damping energy dissipation with friction coefficient under different t.

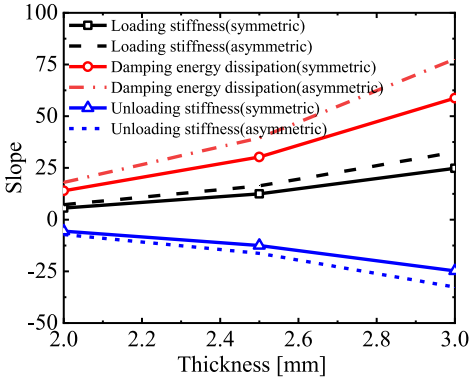

Fig. 20. Loading, unloading stiffness and damping energy slope change with the change of t.

The curves still show an obvious linear trend in both symmetric and asymmetric frictional conditions.

The slopes of the curves of stiffness and damping dissipation with friction coefficient at different t are shown in Fig. 20. It can be seen from the figure that the absolute value of the slope of the change in stiffness and damping dissipation energy gradually increases as the thickness increases, indicating that the sensitivity of stiffness and damping dissipation energy to the friction coefficient is higher at large t. The asymmetry of boundary friction increases the absolute value of the slope of stiffness and damping dissipation change at different t, and the larger the t, the more obvious the increase.

5.3. Analysis of the effect of h on friction

The relationship between stiffness (loading, unloading) and damping dissipation with friction coefficient for different h at $0.75h$ is shown in Figs. 21–23. The effect of the change in cone height on the disc spring stiffness and damping is similar to that of ρ and t. It can be seen that for any h, as the friction coefficient increases, the loading and unloading stiffness gradually increase, and the damping gradually increases. However, the change in cone height has a slightly smaller effect on stiffness and damping compared to ρ and t. In addition, the curves still show an obvious linear trend in both symmetric and asymmetric frictional conditions.

The slope of the curve of stiffness and damping with the friction coefficient for different h is shown in Fig. 24. From the figure, it can be seen that the absolute value of the slope of stiffness change is almost constant with the increase of h, and the absolute value of the slope of damping dissipation energy change rapidly increases, indicating that the damping is more sensitive to the friction coefficient at large h. The asymmetry of boundary friction increases the absolute value of the

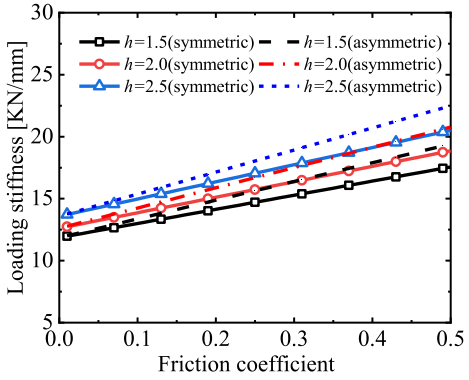

Fig. 21. The change of loading stiffness with friction coefficient under different h.

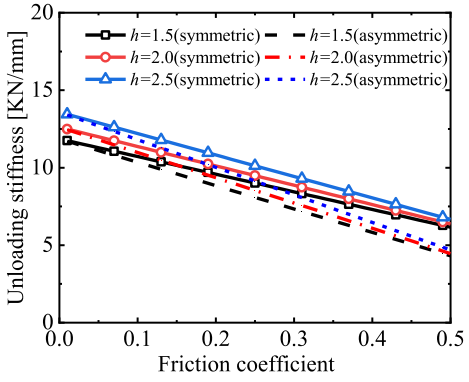

Fig. 22. The change of unload stiffness with friction coefficient under different h.

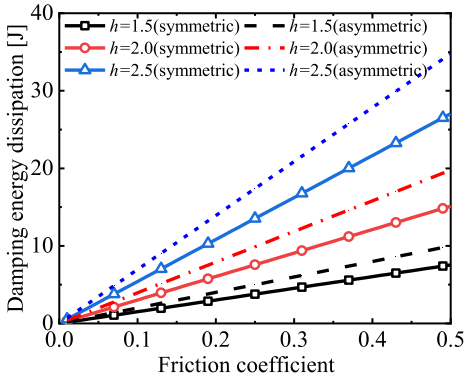

Fig. 23. The change of damping energy dissipation with friction coefficient under different h.

slope of stiffness and damping energy dissipation change for different t, and the increase is greater for larger h.

6. Conclusion

The mechanical model of single-piece disc spring and combined disc springs with asymmetric frictional boundary is derived based on energy method. The theoretical model is validated by FEM and experiments, and it can effectively calculate the load–displacement relationship for different stacking forms of disc springs under symmetric and asymmetric frictional conditions, especially for the damping with good accuracy. And the influence of structural parameters (ρ, t, h) on the mechanical properties of disc springs is investigated, and the main conclusions are:

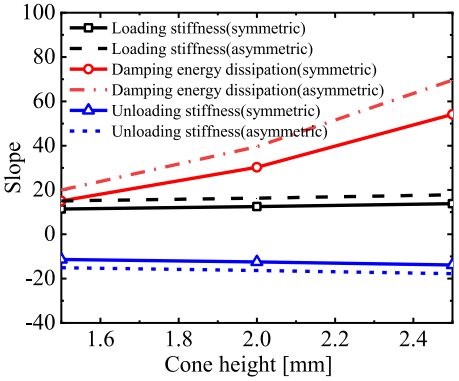

Fig. 24. Loading, unloading stiffness and damping energy slope change with the change of h.

(1) The energy method mechanical model can accurately describe the load–displacement characteristics of disc springs and their combinations under symmetric and asymmetric frictional conditions. In particular, The error between the theoretical and FEM results does not exceed 5% for single-piece disc spring, as well as for the combined disc springs.

(2) The theoretical results are also in good agreement with the experimental results, with the error not exceeding 5% for single-piece disc spring and only 10.87% for three-piece stacking disc springs. Regardless of the different frictional conditions or different combinations, the energy method model is able to capture the changes in mechanical properties due to the asymmetry of the boundary friction.

(3) The structural parameters ρ, t and h of the disc spring can all have an effect on the stiffness and damping. As ρ, t and h increase, the loading stiffness of the disc spring increases and the unloading stiffness decreases, resulting in an increase in damping, and the change in stiffness and damping is nearly linear. The effect of h on stiffness is slightly smaller compared to ρ and t.

(4) Both the structural dimensions of the disc springs and the frictional conditions can affect the sensitivity of the stiffness and damping to the friction coefficient. The larger the t and h, the greater the slope of the change in disc springs stiffness and damping with the friction coefficient, indicating a greater sensitivity to the friction coefficient. In contrast, the larger ρ, the smaller the slope of the change in disc springs stiffness and damping, indicating that it becomes insensitive to the friction coefficient. In addition, the asymmetry of boundary friction can enhance the sensitivity of disc springs stiffness and damping to the friction coefficient.

CRediT authorship contribution statement

Yanfeng Zhou: Writing – original draft, Investigation, Formal analysis, Data curation. **Dan Wang:** Writing – review & editing. **Zhonghui Qiu:** Funding acquisition. **Zixiang Wei:** Conceptualization. **Weifang Chen:** Validation. **Rupeng Zhu:** Validation, Supervision.

Declaration of competing interest

The authors declare that they have no known competing financial interests or personal relationships that could have appeared to influence the work reported in this paper.

Data availability

The data that has been used is confidential.

Acknowledgments

The work described in this paper was fully supported by National Science and Technology Major Project of China (No. J2019-IV-0015-0083).

Appendix A. Derivation of the additional forces of a single disc spring

In the process of compression of a single disc spring, there is a relationship between the deformation δ in the direction of loading and the rotation angle φ of the cross-section as follows

$$\delta = \mathrm{OA}\sin(\theta+\gamma_a)+\mathrm{OB}\sin(\theta+\gamma_b)-\left[\mathrm{OA}\sin(\theta+\gamma_a-\varphi)+\mathrm{OB}\sin(\theta+\gamma_b-\varphi)\right] \tag{A.1}$$

To simplify the derivation process, the geometric constants are introduced according to the structure of the disc spring cross section

$$H = OA\sin\left(\theta+\gamma_a\right)+OB\sin\left(\theta+\gamma_b\right) \tag{A.2}$$

$$V = OA\cos\left(\theta+\gamma_a\right)+OB\cos\left(\theta+\gamma_b\right) \tag{A.3}$$

Expanding Eq.(A.1) by trigonometric functions and substituting Eqs.(A.2) and (A.3), we have

$$\delta = H + V\sin\varphi - H\cos\varphi \tag{A.4}$$

Since the rotation angle φ of the disc spring section around the point O is very small, then we further have

$$\varphi \approx \frac{\delta}{V} \tag{A.5}$$

The slip distances at the upper and lower contact surfaces are

$$l_a = \mathrm{OA}\left[\cos\left(\theta+\gamma_a-\varphi\right)-\cos\left(\theta+\gamma_a\right)\right] \tag{A.6}$$

$$l_b = \mathrm{OB}\left[\cos\left(\theta+\gamma_b-\varphi\right)-\cos\left(\theta+\gamma_b\right)\right] \tag{A.7}$$

Also based on the assumption that φ is very small, the slip distances of the disc spring at the upper and lower edge contact surfaces can be simplified as

$$l_a = \mathrm{OA}\left[\cos\left(\theta+\gamma_a-\varphi\right)-\cos\left(\theta+\gamma_a\right)\right] \approx \mathrm{OA}\sin\left(\theta+\gamma_a\right)\varphi \tag{A.8}$$

$$l_b = \mathrm{OB}\left[\cos\left(\theta+\gamma_b-\varphi\right)-\cos\left(\theta+\gamma_b\right)\right] \approx \mathrm{OB}\sin\left(\theta+\gamma_b\right)\varphi \tag{A.9}$$

After substituting Eq.(A.5) we get

$$l_a = OA\sin\left(\theta+\gamma_a\right)\frac{\delta}{V} = \frac{H_a\delta}{V} \tag{A.10}$$

$$l_b = OB\sin\left(\theta+\gamma_b\right)\frac{\delta}{V} = \frac{H_b\delta}{V} \tag{A.11}$$

Based on the energy balance equations (Eq.(13)), the additional forces required to overcome the friction can be obtained by combining Eqs.(A.10) and (A.11)as

$$\begin{cases} F^*_{f_a}(\delta) = \frac{f_a H_a}{V}F \\ F^*_{f_b}(\delta) = \frac{f_b H_b}{V}F \end{cases} \tag{A.12}$$

Appendix B. Derivation of the additional forces of the disc springs stacked in parallel

In the case of combination with 2 disc springs stacked in parallel, there is only one stacked surface. When the disc springs combination is compressed, the coordinates of points M and N are where $(\Delta x_{\mathrm{PM}}, \Delta y_{\mathrm{PM}})$ is the displacement vector from point P to point M, and the center of rotation is O_1; $(\Delta x_{\mathrm{PN}}, \Delta y_{\mathrm{PN}})$ is the displacement vector from point P to point N, and the center of rotation is O_2.

$$\begin{cases} x_M = x_P + \Delta x_{\mathrm{PM}} \\ y_M = y_P + \Delta y_{\mathrm{PM}} \end{cases} \tag{B.1}$$

$$\begin{cases} x_N = x_P + \Delta x_{\mathrm{PN}} \\ y_N = y_P + \Delta y_{\mathrm{PN}} \end{cases} \tag{B.2}$$

Since l_c is a relative displacement, its magnitude is independent of the choice of coordinate system. For the convenience of expressing calculation, the rotation transformation relationship from point P to points M and N can be extended to the general coordinate system. By decomposing and projecting the rotation arm from point P to the rotation center onto the coordinate axis, and according to the coordinate transformation relations, Eqs.(B.1) and (B.2) can be written as

$$\begin{cases} x_M = x_P - \left[\left(x_P - x_{O1}\right)\left(1-\cos\varphi\right)+\left(y_P - y_{O1}\right)\sin\varphi\right] \\ y_M = y_P + \left[\left(x_P - x_{O1}\right)\sin\varphi - \left(y_P - y_{O1}\right)\left(1-\cos\varphi\right)\right] \end{cases} \tag{B.3}$$

$$\begin{cases} x_N = x_P - \left[\left(x_P - x_{O2}\right)\left(1-\cos\varphi\right)+\left(y_P - y_{O2}\right)\sin\varphi\right] \\ y_N = y_P + \left[\left(x_P - x_{O2}\right)\sin\varphi - \left(y_P - y_{O2}\right)\left(1-\cos\varphi\right)\right] \end{cases} \tag{B.4}$$

For O_1, O_2, there are

$$\begin{cases} x_{O1} = x_{O2} \\ y_{O1} = y_{O2} + \frac{t}{\cos\theta} \end{cases} \tag{B.5}$$

The relative displacement of each stacked surface of the disc springs is

$$l_c = \sqrt{\left(x_M - x_N\right)^2 + \left(y_M - y_N\right)^2} \tag{B.6}$$

Combining Eqs. (B.3) to (B.6), yields

$$l_c = \sqrt{\left(\frac{t}{\cos\theta}\sin\varphi\right)^2 + \left[\frac{t}{\cos\theta}\left(1-\cos\varphi\right)\right]^2} \tag{B.7}$$

Since φ is very small, yields

$$l_c = \frac{t}{\cos\theta}\frac{\delta}{V} \tag{B.8}$$

The following is a further extension to the case of multiple disc springs stacked together, assuming that the deflection of a single disc spring is δ and the load is F. For combination with I disc springs stacked in parallel, it has a total of $(I-1)$ stacked surfaces, and the contact pressure on each stacked surface is $F_e = IF\cos\theta$. If the friction coefficients of each stacked surface are different, the combined damping energy dissipated by the friction of the stacked surfaces is

$$E_{f_c} = \sum_{i=1}^{I-1} E_{f_{ci}} = \left[\sum_{i=1}^{I-1} f_{ci}\right] IF\cos\theta \mathrm{d}l_c \tag{B.9}$$

The total additional work required is

$$E^*_{f_c} = F^*_{f_c}\mathrm{d}\delta_{\mathrm{total}} \tag{B.10}$$

where $F^*_{f_c}$ is the additional load required to overcome the friction of stacked surfaces.

According to the principle of energy conservation ($E_{f_c} = E^*_{f_c}$), jointly established Eqs. (B.9) and (B.10), the combined equivalent load to overcome the friction of the stacked surfaces is

$$F^*_{f_c} = \left[\sum_{i=1}^{I-1} f_{ci}\right] I\frac{t}{V}F \tag{B.11}$$

At this point, the support forces at both the upper and lower contact boundaries are IF. If the individual friction coefficients are not the

same, based on the analysis of a single disc spring, the combined additional load for asymmetric frictional boundaries is

$$\begin{cases} F^*_{f_a} = \sum_{i=1}^{m} \dfrac{f_{ai} H_a}{V} I F \\ F^*_{f_b} = \sum_{i=1}^{n} \dfrac{f_{bi} H_b}{V} I F \end{cases} \tag{B.12}$$

References

[1] G. La Rosa, M. Messina, A. Risitano, Stiffness of variable thickness belleville springs, J. Mech. Des. 123 (2001) 294–299, http://dx.doi.org/10.1115/1.1357162.

[2] N.P. Mastricola, R. Singh, Nonlinear load–deflection and stiffness characteristics of coned springs in four primary configurations, Mech. Mach. Theory 116 (2017) 513–528, http://dx.doi.org/10.1016/j.mechmachtheory.2017.06.006.

[3] S. Kitamura, S. Okamura, K. Takahashi, Experimental study on vertical component seismic isolation system with coned disk spring, in: Volume 8: Seismic Engineering, ASMEDC, Denver, Colorado, USA, 2005, pp. 175–182, http://dx.doi.org/10.1115/PVP2005-71356.

[4] C. Liu, K. Yu, Superharmonic resonance of the quasi-zero-stiffness vibration isolator and its effect on the isolation performance, Nonlinear Dynam. 100 (2020) 95–117, http://dx.doi.org/10.1007/s11071-020-05509-6.

[5] C. Liu, K. Yu, Accurate modeling and analysis of a typical nonlinear vibration isolator with quasi-zero stiffness, Nonlinear Dynam. 100 (2020) 2141–2165, http://dx.doi.org/10.1007/s11071-020-05642-2.

[6] S.H. Ha, M.-S. Seong, S.-B. Choi, Design and vibration control of military vehicle suspension system using magnetorheological damper and disc spring, Smart Mater. Struct. 22 (2013) 065006, http://dx.doi.org/10.1088/0964-1726/22/6/065006.

[7] L. Meng, J. Sun, W. Wu, Theoretical design and characteristics analysis of a quasi-zero stiffness isolator using a disk spring as negative stiffness element, Shock Vibr. 2015 (2015) 1–19, http://dx.doi.org/10.1155/2015/813763.

[8] S. Ramhormozian, G.C. Clifton, G.A. MacRae, G.P. Davet, Stiffness-based approach for Belleville springs use in friction sliding structural connections, J. Constr. Steel Res. 138 (2017) 340–356, http://dx.doi.org/10.1016/j.jcsr.2017.07.009.

[9] D. Castagnetti, F. Dallari, Design and experimental assessment of an electromagnetic energy harvester based on slotted disc springs, Proc. Inst. Mech. Eng. L J. Mater. Des. Appl. 231 (2017) 89–99, http://dx.doi.org/10.1177/1464420716663236.

[10] Y. Zhang, G. Xu, X. Zhang, S. Sha, Design and research of the disc brake of mine hoists for monitoring the disc spring force and positive brake pressure, Meas. Sci. Technol. 30 (2019) 125903, http://dx.doi.org/10.1088/1361-6501/ab3565.

[11] C. Fang, D. Liang, Y. Zheng, M.C.H. Yam, R. Sun, Rocking bridge piers equipped with shape memory alloy (SMA) washer springs, Eng. Struct. 214 (2020) 110651, http://dx.doi.org/10.1016/j.engstruct.2020.110651.

[12] W. Wang, X. Wang, A. Li, Coned disc spring compound vertical isolation: Testing and modelling, J. Earthq. Eng. 26 (2022) 4877–4909, http://dx.doi.org/10.1080/13632469.2020.1850573.

[13] A.J. O, The uniform-section disk spring, Trans. ASME 58 (1936) 305–314.

[14] ISO 19690-1, Disc springs — Part 1: Calculation, 2017, 2017.

[15] GB/T 1972-2005, Disc spring, 2005.

[16] JIS B 2706, Coned disc springs, 2018.

[17] DIN 2092, Disc springs - Calculation, 2006.

[18] G. Curti, R. Montanini, On the influence of friction in the calculation of conical disk springs, J. Mech. Des. 121 (1999) 622–627, http://dx.doi.org/10.1115/1.2829508.

[19] G. Curti, F.A. Raffa, Material nonlinearity effects in the stress analysis of conical disk springs, J. Mech. Des. 114 (1992) 238–244, http://dx.doi.org/10.1115/1.2916937.

[20] N.P. Mastricola, J.T. Dreyer, R. Singh, Analytical and experimental characterization of nonlinear coned disk springs with focus on edge friction contribution to force–deflection hysteresis, Mech. Syst. Signal Process. 91 (2017) 215–232, http://dx.doi.org/10.1016/j.ymssp.2017.01.009.

[21] R. Chen, X. Li, Z. Yang, J. Xu, H. Yang, Nonlinear behavior of disk spring with complex contact state, Sci. Progr. 104 (2021) 00368504211052360, http://dx.doi.org/10.1177/00368504211052360.

[22] R. Chen, X. Li, J. Xu, Z. Yang, H. Yang, Properties analysis of disk spring with effects of asymmetric variable friction, Int. J. Appl. Mech. 13 (2021) 2150076, http://dx.doi.org/10.1142/S1758825121500769.

[23] Ş. Karakaya, Investigation of hybrid and different cross-section composite disc springs using finite element method, Trans. Can. Soc. Mech. Eng. 36 (2012) 399–412, http://dx.doi.org/10.1139/tcsme-2012-0028.

[24] W. Patangtalo, M.W. Hyer, S. Aimmanee, On the non-axisymmetric behavior of quasi-isotropic woven fiber-reinforced composite Belleville springs, J. Reinf. Plast. Compos. 35 (2016) 334–344, http://dx.doi.org/10.1177/0731684415617246.

[25] J. Wang, L. Jian, W. Leng, C. She, Z. Sun, An analytical model for the stiffness of slotted disk springs, Int. J. Appl. Mech. 12 (2020) 2050120, http://dx.doi.org/10.1142/S1758825120501203.

[26] J.H.D. Foard, D. Rollason, A.N. Thite, C. Bell, Polymer composite Belleville springs for an automotive application, Compos. Struct. 221 (2019) 110891, http://dx.doi.org/10.1016/j.compstruct.2019.04.063.

[27] F. Vivio, V. Vullo, Closed form solutions of axisymmetric bending of circular plates having non-linear variable thickness, Int. J. Mech. Sci. 52 (2010) 1234–1252, http://dx.doi.org/10.1016/j.ijmecsci.2010.05.011.

[28] P. Bagavathiperumal, K. Chandrasekaran, S. Manivasagam, Elastic load–displacement predictions for coned disc springs subjected to axial loading using the finite element method, J. Strain Anal. Eng. Des. 26 (1991) 147–152, http://dx.doi.org/10.1243/03093247V263147.

[29] E. Zheng, F. Jia, X. Zhou, Energy-based method for nonlinear characteristics analysis of Belleville springs, Thin-Walled Struct. 79 (2014) 52–61, http://dx.doi.org/10.1016/j.tws.2014.01.025.

[30] D. Zhu, F. Ding, H. Liu, S. Zhao, G. Liu, Mechanical property analysis of disc spring, J. Braz. Soc. Mech. Sci. Eng. 40 (2018) 230, http://dx.doi.org/10.1007/s40430-018-1152-2.

[31] R. Chaturvedi, M. Trikha, K.R.Y. Simha, Theoretical and numerical analysis of stepped disk spring, Thin-Walled Struct. 136 (2019) 162–174, http://dx.doi.org/10.1016/j.tws.2018.12.003.

[32] S. Ozaki, K. Tsuda, J. Tominaga, Analyses of static and dynamic behavior of coned disk springs: Effects of friction boundaries, Thin-Walled Struct. 59 (2012) 132–143, http://dx.doi.org/10.1016/j.tws.2012.06.001.

[33] G. Curti, M. Orlando, G. Podda, Vereinfachtes Verfahren zur Berechnung von Tellerfedern, Draht 31 (1980) 789–792.

[34] G. Curti, R. Montanini, On the influence of friction in the calculation of conical disk springs, J. Mech. Des. 121 (1999) 622–627, http://dx.doi.org/10.1115/1.2829508.

[35] M.S. Blanter, I.S. Golovin, H. Neuhauser, H.R. Sinning, Internal friction in metallic materials, A Handb. 540 (2007) 1–144.

[36] P.J. Blau, ASM Handbook, Volume 18 - Friction, Lubrication, and Wear Technology, ASM International.

[37] G. Curti, M. Orlando, New calculation of coned annular disk spring, in: Mechanical Engineering, Vol. 10017, ASME-AMER Soc Mechanical Eng 345 E 47TH ST, New York, NY, 1977, p. 104.

[38] G. Curti, Geschlitzte Tellerfedern. Spannungen und Verformungen, 1981.

[39] G. Curti, R. Montanini, Theoretical, numerical and experimental analysis of conical disk spring, in: XXV AIAS Gall. Lecce Sept. 1, 1996, p. 573.

[40] X. Li, R. Chen, Z. Yang, H. Yang, J. Xu, Static behavior analysis of disc spring considering variable static friction coefficient, Proc. Inst. Mech. Eng. C J. Mech. Eng. Sci. 235 (2021) 5583–5593, http://dx.doi.org/10.1177/0954406220985552.

[41] N.P. Mastricola, Nonlinear Stiffness and Edge Friction Characterization of Coned Disk Springs, The Ohio State University, 2016, https://etd.ohiolink.edu/apexprod/rws_olink/r/1501/10?clear=10&p10_accession_num=osu1480346443676492. (Accessed 11 May 2023).

[42] X. Du, C. Liao, B. Gan, Y. Zhang, L. Xie, H. Zhang, Analytical modeling and experimental verification for linearly gradient thickness disk springs, Thin-Walled Struct. 167 (2021) 108153, http://dx.doi.org/10.1016/j.tws.2021.108153.